ISSN: 0067-2904

A Comparative Analysis of Zernike and Karhunen-Loeve Polynomials for Wave-front Correction in Modal Adaptive Optics Systems

Raaid Nawfee Hassan
Department of Astronomy and Space, College of Science, University of Baghdad, Baghdad, Iraq.

Received: 18/1/2025 Accepted: 9/7/2025 Published: 30/6/2026

ABSTRACT

This work employed the Zernike and Karhunen-Loeve polynomials in the adaptive optics (AO) systems to correct wave-front aberrations. The present work uses MATLAB-based program for simulating wave-front distortion correction with the use of the Modal AO method. Wave-front aberrations were represented by a modified von Karman turbulence model; numerical simulations and analyses were performed. The Zernike polynomials higher values of SNR and Strehl ratios, lower values of RMSE, variance, and covariance in comparison to Karhunen-Loeve polynomials modes, proved the superiority of the Zernike polynomials in correcting wave-front distortion. The present work provides valuable insights into the quality and performance metrics of the Karhunen-Loeve and Zernike modes, with a focus on gaining a more detailed understanding of the different aberration modes for enhancing wave-front corrections in optical systems.

Keyword: Zernike polynomials, Karhunen-Loeve Polynomials, Modal adaptive optics, PSF, and Modified von Karman Turbulence.

تحليل مقارن لمتعددات حدود Zernike و Karhunen–Loeve لتصحيح جبهة الموجة في أنظمة البصريات التكيفية النمطية

رائد نوفي حسان
قسم الفلك والفضاء، كلية العلوم، جامعه بغداد، بغداد، العراق

الخلاصه

استخدم هذا العمل متعددات حدود زيرنيك وكارهونين–لوف في أنظمة البصريات التكيفية (*AO*) لتصحيح انحرافات جبهة الموجية. يستخدم العمل الحالي برنامجًا قائمًا على *MATLAB* لمحاكاة تصحيح تشوه جبهة الموجية باستخدام طريقة *AO* النمطية. تم تمثيل انحرافات جبهة الموجية بواسطة نموذج اضطراب فون كارمان المعدل؛ تم إجراء عمليات محاكاة وتحليلات عددية. أثبتت القيم الأعلى لنسبة الإشارة إلى الضوضاء ونسب سترايل في متعددات حدود زيرنيك، والقيم المنخفضة لـ *RMSE*، والتباين، والتغاير مقارنة بأوضاع متعددات حدود كالرهونين–لوف، تفوق متعددات حدود زينيك في تصحيح تشوه جبهة الموجية. يوفر العمل الحالي رؤى قيمة حول مقاييس الجودة والأداء لأنماط كالرهونين–لوف وزيرتيك، مع التركيز على اكتساب فهم أكثر تفصيلاً لأوضاع الانحراف المختلفة لتعزيز تصحيحات الجبهة الموجية في الأنظمة البصرية.

*Email: raaid.hassan@sc.uobaghdad.edu.iq

1. Introduction

Ground-based telescopes can achieve theoretical diffraction-limited resolution through the use of Adaptive Optics (AO) to compensate for the blurring effect of the Earth's atmosphere. The largest telescopes and most innovative scientific equipment, combined with the high angular resolution provided by AO, make this combination a critical tool for the purpose of studying and understanding the universe [1].

In the 21st century, effective communication by the American National Standards Institute (ANSI) and the International Organization for Standardization (ISO) was promoted through the Zernike polynomials developments and the standardization of several Zernike sets [2].

Zernike polynomials are extensively used because of their exceptional mathematical properties. They are orthogonal over a unit circle. Because of this orthogonality, wave-front function expansion coefficients are independent of the number of terms. This enables convenient mathematical manipulations of wavefronts, such as addition, subtraction, translation, rotation, and scaling. Also, they efficiently represent common optical errors, such as astigmatism, coma, and spherical aberration, which ease the classifications and quantifications of wave-front aberrations [3]. Moreover, the evaluation of the image quality of an optical system using the Zernike polynomials is easy since the system point spread function(PSF) can be analytically computed from the Zernike expansion coefficients of the wave-front aberrations based on the (extended) Nijboer–Zernike theory [4]. Zernike and Karhunen-Loeve (KL) polynomials have been utilized to simulate atmospheric turbulence, taking into consideration temporal as well as spatial effects on observed images. In addition to that, due to their orthonormality and statistical independence, KL polynomials have been utilized in favor of the Zernike polynomials [5].

To effectively correct or minimize various types of aberration modes that are introduced by atmospheric turbulence, it is essential to first capture and quantitatively describe their characteristics [6]. For this purpose, the wave aberration function works suitably, as it provides a comprehensive description of the combined impact of the optical system on light as it passes through every point within the aperture of the telescope [7].

The von Karman model presents the nature of the wave-front perturbations caused by atmospheric turbulence [8]. This model is commonly used in simulations of imaging through atmospheric turbulence and is backed by a number of experimental studies. It directly causes phase fluctuations by attributing the wave-front perturbations to changes in the atmosphere's refractive index [9].

The study demonstrates how to choose the ideal polynomial basis functions for AO systems for effective astronomical observations and improved image quality. Several studies have investigated the use of Zernike or KL polynomials individually in adaptive optics, often demonstrating advantages unique to each. However, most prior research lacks a systematic, metric-based comparison of both bases under the same simulation conditions. This research aims to fill that gap by evaluating the comparative performance of both basis sets across multiple quality metrics under identical, physically realistic conditions.

The originality of this paper lies in its quantitative performance evaluation of Zernike and KL polynomials under realistic atmospheric turbulence modeled by a modified von Karman spectrum. It further distinguishes itself by applying multiple image quality metrics such as Strehl, Signal to Noise Ratio (SNR), Root Mean Square Error (RMSE), variance, and covariance. This comprehensive comparison provides clear, evidence-backed

recommendations for AO system design, which were not previously established in such an integrated manner. The efficacy of a modified von Karman turbulence model in simulating atmospheric effects on wavefronts was examined to better apprehend the accuracy and applicability of this model in representing real-world conditions for Modal AO systems.

2. Light Beam Propagation

The beam propagation technique is widely used to numerically simulate light propagation through nonlinear, inhomogeneous, and anisotropic materials, such as wave-guiding structures with gentle variations along propagation direction. With this technique, solutions are calculated in very small increments, taking into consideration the separate linear and nonlinear (or non-deterministic) steps [10].

The profiled electromagnetic beam is where we start at $z = 0$. The profiled beam travels from $z\ to\ z + \Delta z$, covering the first longitudinal increment (Δz) in our case, which is Gaussian. The field experiences the familiar Fresnel-Kirchhoff diffraction integral across this distance (Δz), substituting Δz for z in the following way [11][12]:

$$U(x_i, y_i) = \iint_{-\infty}^{\infty} U(x_0, y_0) \exp\left(j\frac{k}{2z}((x_i, x_0)^2 + (y_i, y_0)^2)\right) dx_0 dy_0 \quad (1)$$

In which $U(x_0, y_0)$ represents the input profiled beam, $U(x_i, y_i)$ represents the field following distance Δz, k represents the unbounded wave number.

Therefore, phase perturbations due to turbulence-induced fluctuations in the refractive index following a distance of Δz are represented by the multiplication of the field by a phase function $e^{(i\varphi(x,y))}$ as [13][14]:

$$U_{out}\ (x_i, y_i) = U_{in}\ (x_i, y_i) e^{i\varphi\ (x_i, y_i)} \quad (2)$$

Where: $U_{out}\ (x_i, y_i)$ represents the field amplitude immediately following the random phase screen, and $U_{in}\ (x_i, y_i)$ represents the field amplitude before the random phase screen. The procedure above is repeated until the field has traveled the required distance.

The propagation path in the case of a single-phase screen could be divided into two parts: (a) from the phase screen to the observation plane at $z = L$, and (b) from the phase screen to input profiled Gaussian beam [15]. One way to represent a single-phase screen is as a particular type of extended phase screen. Complexity and accuracy must be balanced while working with the extended-phase screen, which depicts a broad range of turbulence [16] [17]. Thus, the incremental diffractive distance (Δz) reduces with the increased phase screen count for a given propagation distance, leading to longer processing times. To better represent atmospheric turbulence across an extensive medium, $\Delta z \to 0$, an infinite number of phase screens is the ideal condition [18][19].

3. Model Approach

The estimated functions serve as coefficients of the aperture function in a Modal representation. A set of functions is used to represent the wavefront; these functions are all applicable over the entire aperture. It is necessary for both functions to be linearly independent in order to represent the phase as [20]:

$$\varphi(x, y) = \sum_{k=1}^{K} a_k\, Z_k(x, y) \quad (3)$$

Where: a_k is the coefficients and Z_k is the function, Zernike or KL polynomials, that will be discussed to approximate the wave-front.

4. Zernike Polynomials

The power series terms in the Zernike polynomial expansion include proper normalization factors. The standard normalized low-order Zernike polynomials are defined over the unit circle. The classical and most widely utilized Zernike polynomials, in this study, have been normalized over a circular domain by Noll [21]. These polynomials have the following precise definitions [22] [23]:

$$Z_{even\ j} = \sqrt{n+1}\ R_n^m\ (r)\ \sqrt{2}\cos m\theta \tag{4}$$

$when\ m \neq 0$

$$Z_{odd\ j} = \sqrt{n+1}\ R_n^m\ (r)\ \sqrt{2}\sin m\theta \tag{5}$$

$when\ m \neq 0$

$$Z_j = \sqrt{n+1}\ R_n^0\ (r)\ , when\ m = 0 \tag{6}$$

Where the radial function:

$$R_n^m(r) = \sum_{s=0}^{(n-m)/2} \frac{(-1)^s}{s!\left[\frac{n+m}{2}-s\right]!\left[\frac{n+m}{2}-s\right]!}\ r^{n-2s} \tag{7}$$

n and m are frequently used integrals and satisfy $m \leq n, n-|m| = even$. Index j represents a mode ordering number and is a function of n and m. Each type of aberration mode can be illustrated as in Figure 1.

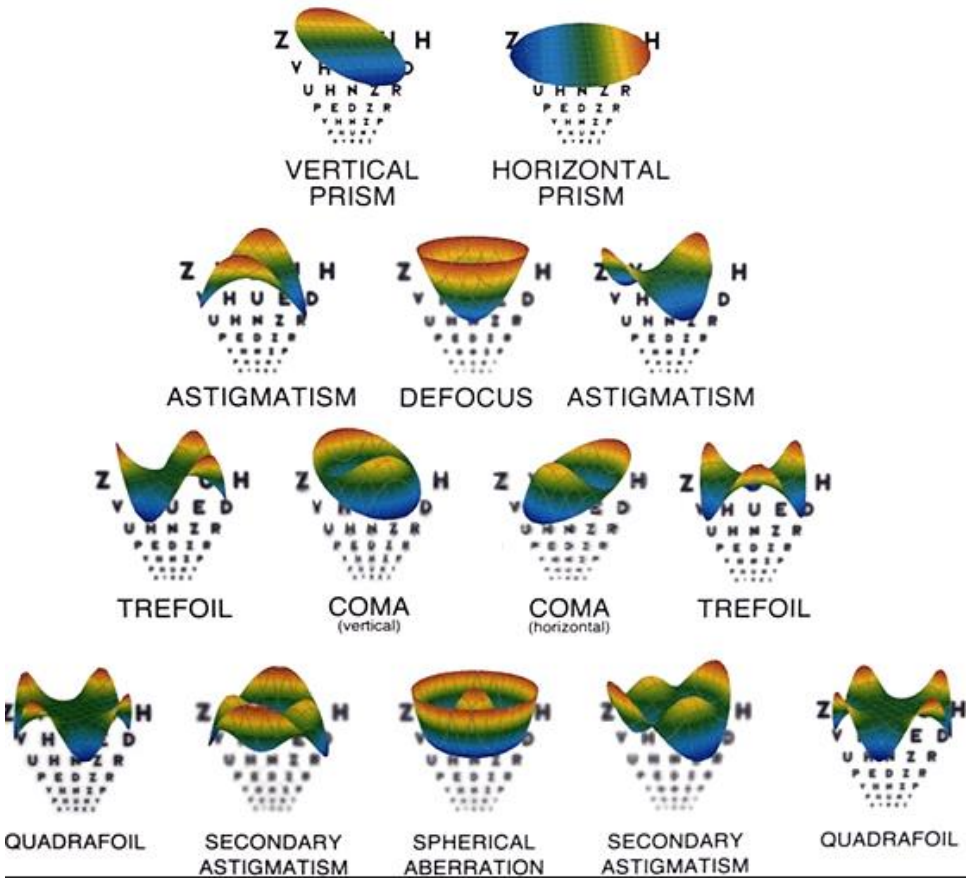

Figure 1: Typical circle Zernike polynomials [24].

5. Karhunen-Loeve polynomials

Zernike polynomials make up the Karhunen-Loeve (KL) polynomials, yet their coefficients are statistically independent. Comprehension of atmospheric turbulence,

represented by the Kolmogorov model depending on Kolmogorov statistics [25] [26], requires an understanding of this feature. The basis of KL functions is Zernike polynomial expansion. Using this method, KL equations may be reduced to a system of linear algebraic equations that can be analytically defined with regard to the hypergeometric function for matrix elements [27]. The specified KL polynomials are [28][29]:

$$K_p(\rho,\theta) = \sum_{j=1}^{N} b_{p,j} Z_j \quad (8)$$

Where: $b_{p,j}$ is the constructing matrix of KL polynomials (which could be found in the study of Hassan et al. [5]), and N represents the number of Zernike orders where KL order j is represented. Table 1 contains KL aberration modes up to the 4th order that were used in our research.

Table 1: Karhunen-Loeve polynomials up to 4th order [5]

Order	Aberration mode
K1	Z_1
K2	$b_{2,2}Z_2+ b_{2,7}Z_7 +b_{2,16}Z_{16}$
K3	$b_{3,3}Z_3+ b_{3,8}Z_8 +b_{3,17}Z_{17}$
K4	$b_{4,5}Z_5+ b_{4,12}Z_{12} +b_{4,23}Z_{23}$
K5	$b_{5,6}Z_6+ b_{5,13}Z_{13} +b_{5,24}Z_{24}$
K6	$b_{6,4}Z_4+ b_{6,11}Z_{11} +b_{6,22}Z_{22}$
K7	$b_{7,9}Z_9+ b_{7,18}Z_{18} +b_{7,31}Z_{31}+b_{7,48}Z_{48}$
K8	$b_{8,10}Z_{10}+ b_{8,19}Z_{19} +b_{8,32}Z_{32}+b_{8,49}Z_{49}$
K9	$b_{9,2}Z_2+ b_{9,7}Z_7 +b_{9,16}Z_{16}+b_{9,29}Z_{29}+b_{9,46}Z_{46}$
K10	$b_{10,3}Z_3+ b_{10,8}Z_8 +b_{10,17}Z_{17}+b_{10,30}Z_{30}+b_{10,47}Z_{47}$
K11	$b_{11,14}Z_{14}+ b_{11,25}Z_{25} +b_{11,40}Z_{40}+b_{11,64}Z_{64}$
K12	$b_{12,15}Z_{15}+ b_{12,26}Z_{26} +b_{12,41}Z_{41}+b_{12,65}Z_{65}$
K13	$b_{13,5}Z_5+ b_{13,12}Z_{12} +b_{13,23}Z_{23}+b_{13,38}Z_{38}+b_{13,62}Z_{62}$
K14	$b_{14,6}Z_6+ b_{14,13}Z_{13} +b_{14,24}Z_{24}+b_{14,39}Z_{93}+b_{14,63}Z_{63}$
K15	$b_{15,4}Z_4+ b_{15,11}Z_{11} +b_{15,22}Z_{22} +b_{15,37}Z_{37}+b_{15,56}Z_{56}+b_{15,79}Z_{79}$

Atmospheric Turbulence

An introduction to atmospheric turbulence is given in this section, with a particular emphasis on the modified von Karman phase turbulence model. The numerical generation regarding random phase screens that illustrate random turbulence behavior across a thin transverse layer in the propagation direction is explored [30]. There is a chance that the properties of optical waves passing through atmospheric turbulence would vary significantly, which could impair system performance. Three parameters are essential in standard turbulence modelling to describe the behavior regarding atmospheric turbulence: the outer (L_0) and inner (l_0) scales of turbulence eddies and the refractive index structure parameter (C_n^2) that indicates the strength related to atmospheric turbulence [31].

6. Von Karman Modeling

To make the Tatarski spectrum valid for both the outer and inner scale parameters, von Karman adjusted it in a way to be finite for $k < 1/L_0$. Modified von Karman Spectrum's power spectrum density is provided by [32]:

$$\varphi_n(k) = 0.033C_n^2 \frac{\exp\left(-\frac{k^2}{k_m^2}\right)}{(k^2 + k_0^2)^{\frac{11}{6}}} \quad 0 \le k \le \infty \tag{9}$$

The medium structure constant is denoted by C_n^2 by the above equation: the equivalent wavenumber for the inner scale is $k_m = 5.92/l_0$, the wavenumber for the outer scale is $k_0 = 2\pi/L_0$, and the unbounded non-turbulent wave number in the medium is k. Here, $\varphi_n(k)$ represents the medium's refractive index's PSD (power spectral density). One of its main advantages is that this model is integrable at k=0 and includes both outer and inner scales [33].

7. Phase Screen Generation

Examining how to utilize a discrete grid is to create a phase screen that replicates statistical features of phase fluctuations brought on through turbulent atmospheric conditions, and how to employ Fast Fourier Transform (FFT) methods to generate a phase screen from the specified spectrum. A phase screen's main goal is to simulate the disturbances of the random phase that result from unpredictable fluctuations in the refractive index during extended atmospheric turbulence [34]. Planar or extended, the generated random phase screen is determined by several parameters, including the inner and outer scales (l_0 and L_0), the incremental spatial frequencies Δk_x, Δk_y, and C_n^2 (or Fried parameter r_0). Creating a series of random complex numbers (with a Gaussian distribution) on a selected grid involves starting with the modified von Karman spectrum model with the given parameters and utilizing a standard scheme depending upon the generation of the Fourier transform. The phase screen is obtained through an inverse Fourier transform after the random numbers are multiplied by the phase power spectrum's square root, as in Equation (10). Depending on the modified von Karman spectrum model, the real part of the result is regarded as a random phase function $\varphi(x,y)$ owing to the atmospheric fluctuations. In 2-D, the discrete phase distribution is written as [18]:

$$\varphi_{ij} = Re\left\{IFFT\left((a+ib)\sqrt{\varphi_n \Delta k_x \Delta k_y}\right)\right\} \tag{10}$$

Inverse fast Fourier transform operation (IFFT) is represented by a and b, which are random numbers created to suitably simulate the modified von Karman phase's random noise-like properties, $\varphi_n(k)$, as in Equation (9).

8. Numerical Simulations, Results, and Discussion

The effectiveness of two orthogonal functions in the Modal AO systems for wave-front correction was investigated using a numerical computer simulation, which used Zernike aberration modes for computing KL polynomials that were useful for the wave-front aberrations representation and analysis in the optical systems. A phase screen, which replicated the statistical properties of phase fluctuations that occurred due to turbulent atmospheric conditions, was generated using a modified von Karman model. The numerical simulation for profiled wave-front beam propagation over a turbulent medium, the atmosphere, was presented in this section. The detailed steps of the flowchart for the computer simulation, focusing on efficient wavefront reconstruction and compensation using two orthogonal functions, are presented in Figure 2.

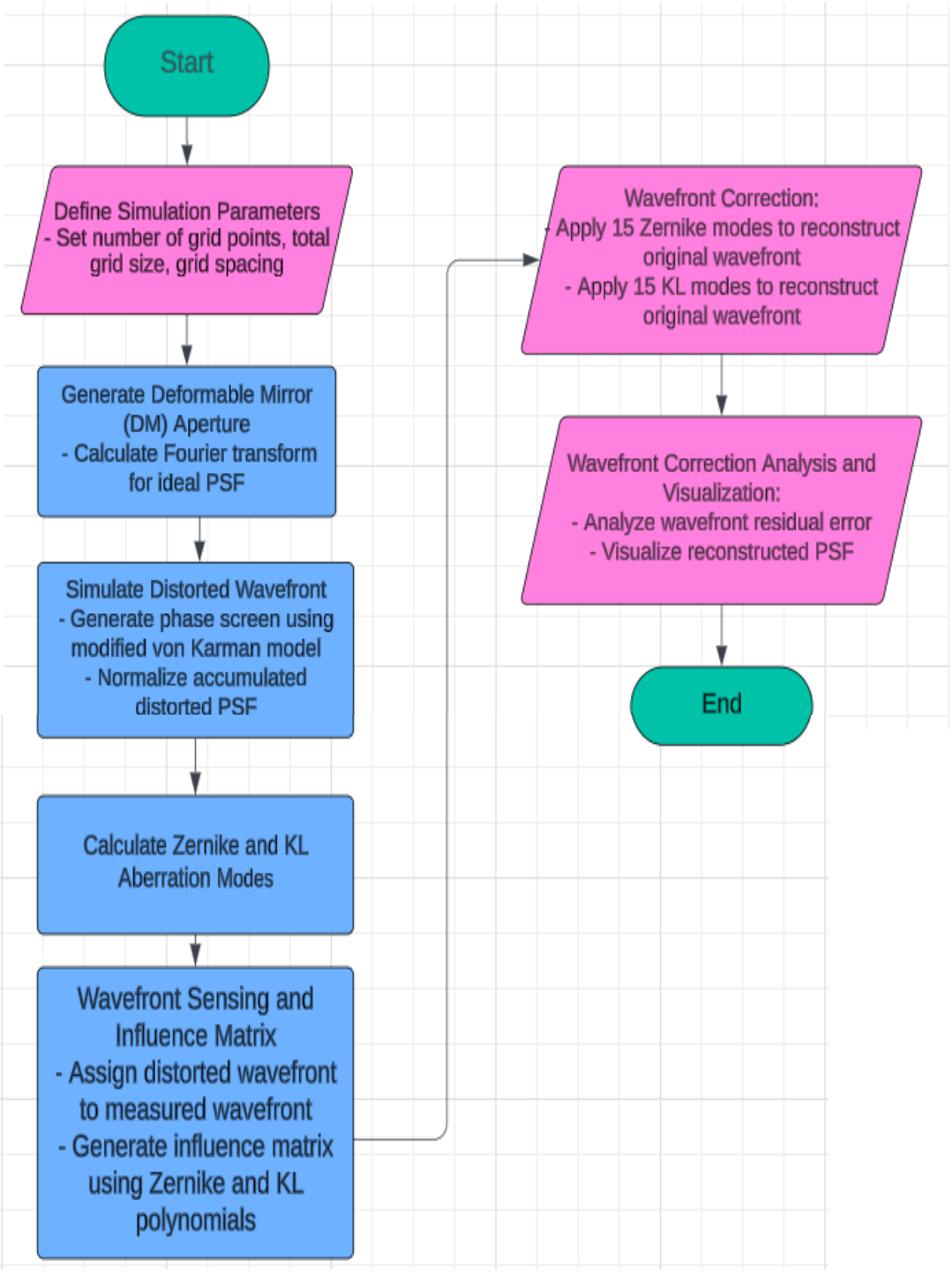

Figure 2: Flowchart of the computer simulation process.

9. 1. Initialization and Parameter Setup:

The simulation parameters, the number of grid points, total grid size, and grid spacing were defined, as in Table 2.

Table 2: Includes All Basic Simulation Parameters.

Parameter	Value	Description
Grid size (N)	256	Spatial resolution
Wavelength (λ)	550 nm	Central observing wavelength
Turbulence model	Modified von Karman	Atmospheric phase perturbation model
Number of modes	15	Zernike/KL modes used in correction
r_0	0.1 m	Fried parameter
L_0	25 m	Outer scale of turbulence

9. 2. Deformable Mirror (DM) and Ideal Point Spread Function (PSF) Generation:

An amplitude pattern (circular deformable mirror (DM) aperture) for the wavefront was generated, as shown in Figure 3, for which the Fourier transform was calculated to create the ideal Point Spread Function (PSF), shown in Figure 4.

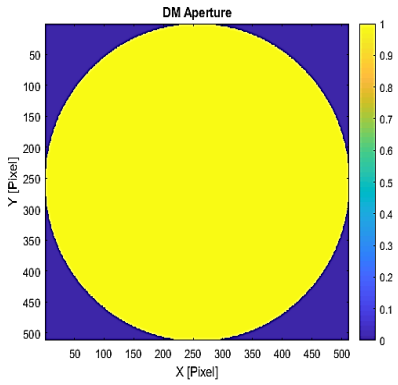

Figure 3: The DM Aperture.

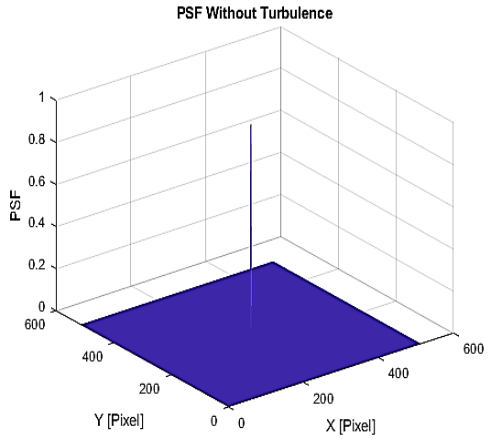

Figure 4: The Ideal PSF of the Optical System.

9. 3. Distorted Wave-front Simulation and its PSF:

The phase screen was generated by simulating a distorted wavefront with a modified von Karman turbulence model's PSD, as shown in Figure 5. The accumulated distorted PSF was normalized, as in Figure 6. The Strehl Ratio was calculated as the ratio of the highest value in the ideal PSF to the highest in the distorted PSF, resulting in a Strehl Ratio of 0.0834.

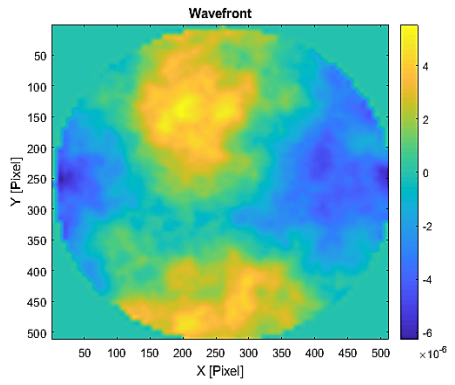

Figure 5. The Original Distorted Wavefront.

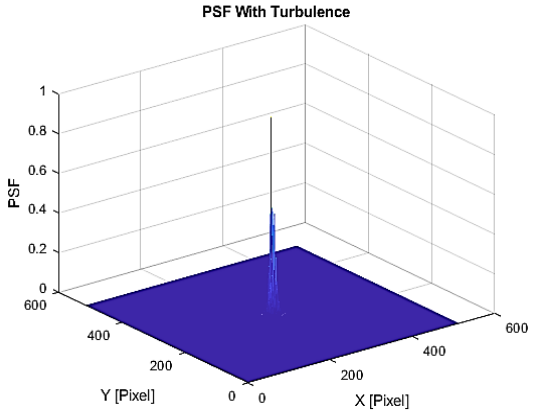

Figure 6. The Normalized Accumulated Distorted PSF.

9.4. Calculation of the Required KL Aberration Modes:

The KL aberration modes can be represented according to Table 1, and they are shown in Figure 7.

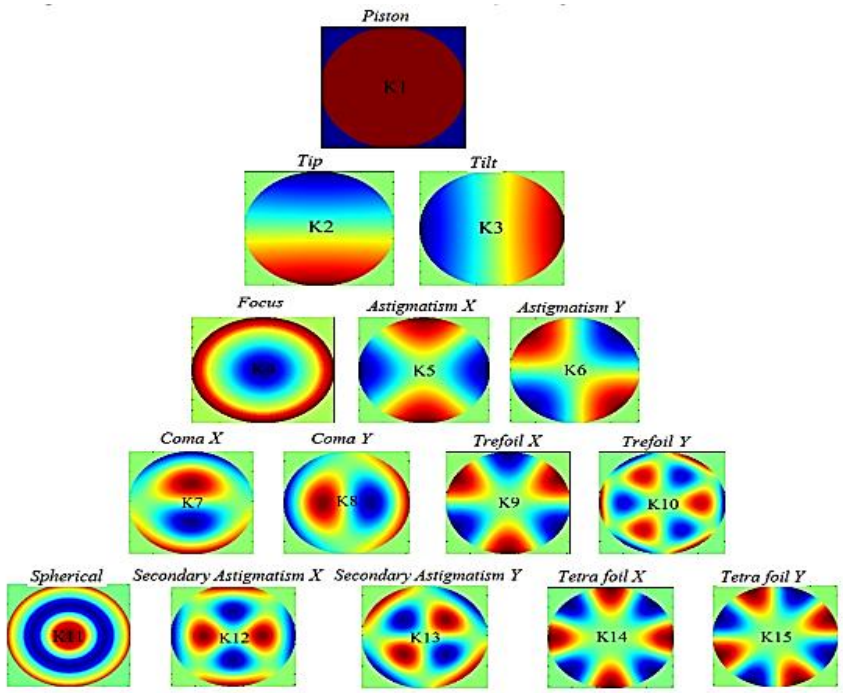

Figure 7: Graphical Representation of the KL Polynomials up to the 4th Order

9.5. Wave-front Sensing and Influence Matrix:

The distorted wavefront was assigned to the measured wavefront. An influence matrix, which is the interaction of deformable mirror actuators with the wavefront, was generated for Modal AO using the Zernike and KL polynomials. Figure 8 represents the sum of 15 Zernike aberration modes, and Figure 9 represents the sum of 15 KL aberration modes. Zernike and KL polynomials are a set of orthogonal basis functions that were used in Modal AO to control the deformable mirror surface to represent the wave-front distortion. The control signals for the deformable mirror actuators were calculated using these two functions. This allows for the correction of a wide range of wave-front aberrations.

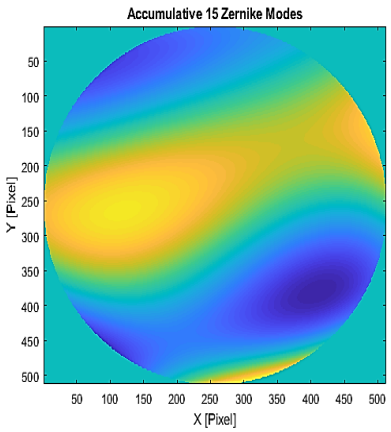

Figure 8: The Accumulative 15 Zernike's Aberration Modes.

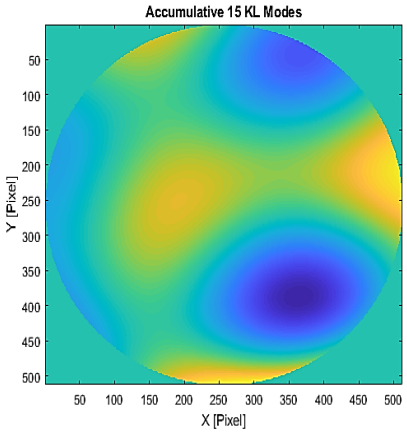

Figure 9: The Accumulative 15 KL's Aberration Modes.

It can be noted from Figures 7 and 8 that the Zernike modes give a smoother representation of the wave-front aberrations, and this is due to their well-established use in practical AO systems. KL modes, although they offer better statistical representation of the wave-front error, show more variability and sensitivity to certain characteristics of the observed wavefronts.

8.6. Wave-front Correction:

To reconstruct the original wavefront shown in Figure 5, wave-front correction was calculated by applying the accumulative 15 Zernike aberration modes, shown in Figure 8, to the measured wavefront. Figure 10 shows the reconstructed wavefront. Still, there remains a relatively low wave-front error between the reconstructed and original wavefront, as shown in Figure 11. This low error shows that the Zernike modes have successfully reduced most of the wave-front distortions. This result proves that the Zernike modes are suitable to be applied for applications where high wave-front correctness is required.

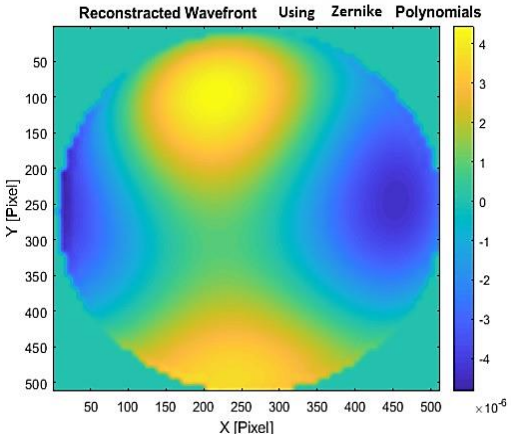

Figure 10: The reconstructed wavefront using 15 Zernike's aberration modes.

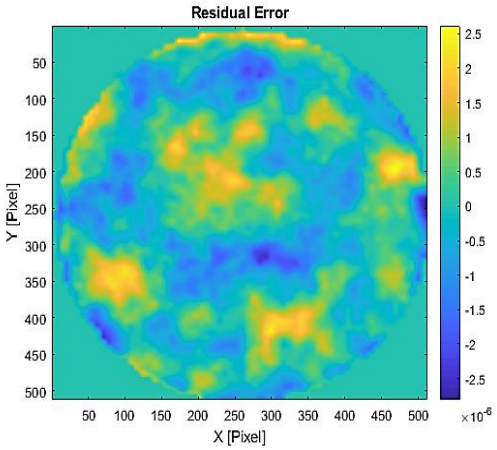

Figure 11: The difference between the reconstructed wavefront and original

The accumulative 15 KL aberration modes, shown in Figure 9, were employed to calculate the wave-front correction for reconstructing the original wave-front (shown in Figure 5). The reconstructed wavefront is shown in Figure 12. The remaining wave-front error between the reconstructed and original wavefront can be noted from Figure 13.

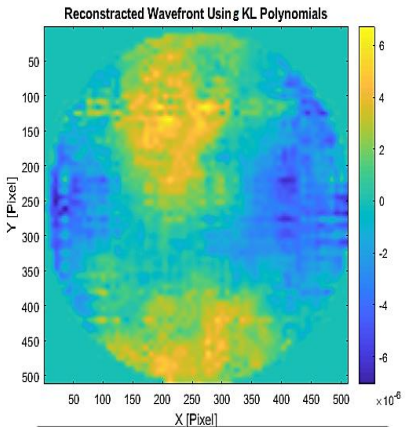

Figure 12: Represents the reconstructed wavefront using 15 KL's aberration modes.

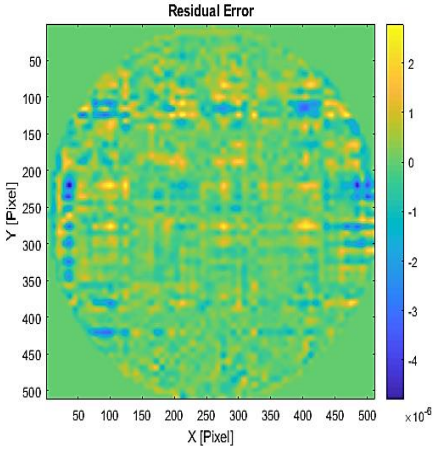

Figure 13: The difference between the reconstructed wavefront and original wavefront.

Comparing Figures 12 and 13, it can be noted that the wave-front residual error using the Zernike modes is lower than that using the KL modes, indicating that the Zernike modes offer more accurate wave-front correction, giving better overall image quality in practical applications. Zernike modes may minimize the overall variance; they are not as effective as the KL modes in correcting certain types of wave-front aberrations. This concludes that the Zernike modes are more accurate than the KL modes to get good image quality.

8.7. Analysis and Visualization of PSFs:

The reconstructed PSF is shown in Figure 14. Strehl ratio, covariance, RMSE, and variance were plotted against individual aberration no. modes (for both Zernike and KL modes), as shown in Figure 15. Figure 16 shows the plots of Strehl ratio, covariance, RMSE, and SNR against accumulative aberration no. modes.

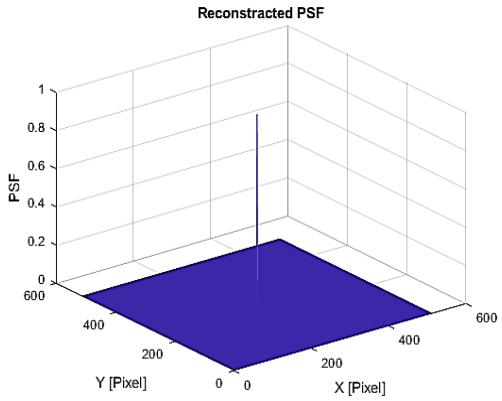

Figures 14. The Reconstructed PSF.

The Strehl ratio measures the quality of the optical system; high values indicate good performance. The covariance represents the spread of the data points. Low values indicate less spread. The Root Mean Square Error, or RMSE, measures the difference between actual and calculated values; low RMSE values indicate good accuracy.

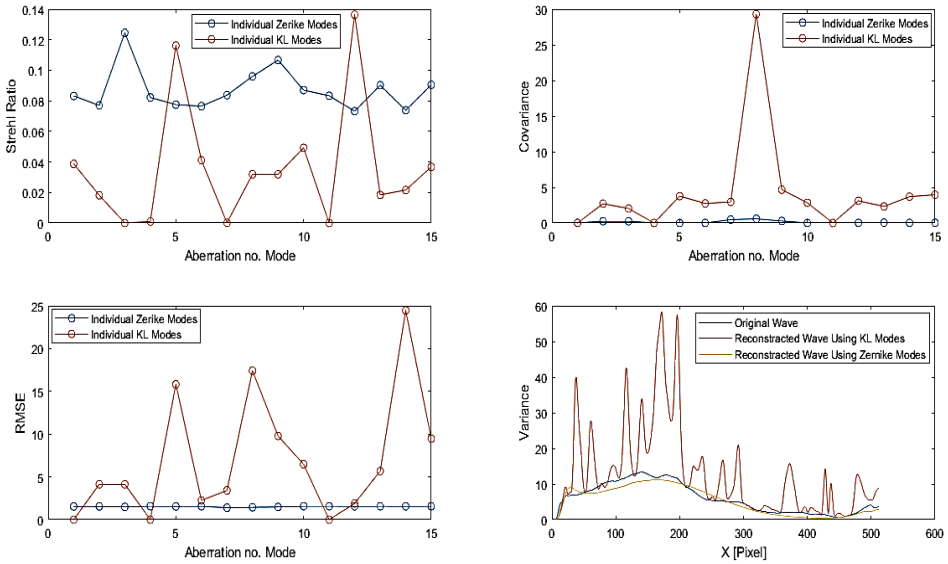

Figures 15: (a) Strehl Ratio, (b) Covariance, (c) RMSE as a function of individual aberration no. modes (for both Zernike and KL modes), and (d) Variance.

From Figure. 15a, it can be noted that the Zernike modes generally have higher Strehl Ratio values compared to KL modes. Also, there is major variability in the Strehl Ratio values for KL modes compared to the Zernike modes. This indicates that the Zernike modes perform better than the KL modes. Figures (15b and 16b) demonstrate that the individual and accumulative Zernike modes have lower covariance values than those of the KL modes. Both individual and accumulative Zernike modes are of good accuracy, as indicated by their lower RMSE values than those of the KL modes, as seen in Figures (15c and 16c). The individual KL modes reveal high variation in the variance values compared to those of the Zernike modes, as seen in Figure 15d. This indicates that the Zernike modes match the original wave-front data well. Signal-to-Noise Ratio (SNR) measures the signal quality. The higher the value, the better the quality of the signal. Figure (16d) shows that the accumulative Zernike aberration modes are of better performance than the accumulative KL modes. The results showed higher Strehl Ratio values, lower covariance values, and lower RMSE values for the Zernike modes compared to those of the KL modes.

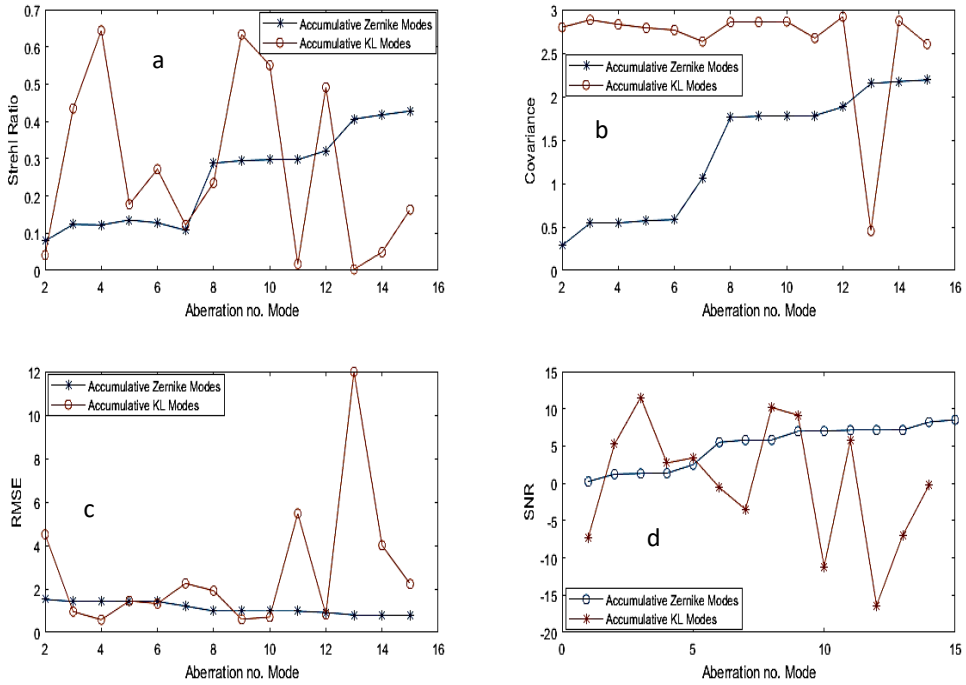

Figures 16: (a) Strehl Ratio, (b) Covariance, (c) RMSE, and (d) SNR as a function of accumulative aberration no. modes (for both Zernike and KL modes).

It is important to consider the computational cost associated with implementing Zernike and KL polynomials. In our simulations, the average processing time for reconstructing wavefronts using KL modes was higher due to the additional step of Eigen-decomposition required to generate the KL basis. Zernike polynomials, being analytically defined, were computationally more efficient. This makes Zernike a preferred choice in real-time AO systems where speed is critical. In this study, 15 modes were selected based on a balance between computational complexity and correction accuracy. Increasing the number of modes improves correction accuracy but also increases computational burden and potential fitting error in the presence of noise. We observed diminishing returns in image quality improvement beyond 15 modes.

The superior performance of Zernike polynomials can be attributed to the nature of the atmospheric turbulence simulated by the modified von Karman model, which introduces low-

order aberrations that are well captured by Zernike modes. Furthermore, the absence of noise in the simulation and the limited number of modes may also favor Zernike. This observation aligns with previous studies where Zernike was found to be more robust for low-to-moderate order aberration correction under similar turbulence models. Our study assumes that the von Karman model accurately represents atmospheric turbulence, though it may not cover all real-world conditions, particularly in dynamic or localized turbulence. Simulations were used to assess the performance of Zernike and KL polynomials under ideal conditions, such as perfect system alignment, which may not reflect actual usage. However, limitations include the resolution of the simulations, constrained by computational resources, and the limited number of actuators in the deformable mirror, both of which could affect accuracy in correcting higher-order aberrations in real-world applications.

Conclusion

The results from the numerical simulation and analyses clearly show the effectiveness of wave-front aberration studies in Modal adaptive optics systems. Information about the quality and performance measurements was obtained using two orthogonal functions, Zernike and Karhunen-Loeve polynomials, for wave-front correction. Both polynomials were used to evaluate the system's ability to correct aberration, providing a comparative analysis of their effectiveness in enhancing wave-front reconstruction and reducing the residual errors.

Zernike aberration modes were proved to be more beneficial in correcting wave-front distortions compared to Karhunen-Loeve modes. As evidenced by their higher Strehl Ratio and SNR values, which indicate better image quality and improved optical performance, and lower variance, covariance, and RMSE values. These results indicate the importance of knowing and understanding the properties and possible implementations of different aberration modes to improve wave-front distortion corrections in optical systems. This research did not study the possible benefits of hybrid AO systems that combine zonal (Zernike) and modal (Karhunen-Loeve) methods. Future work might investigate whether such hybrid systems provide high correction accuracy by exploiting the strengths of both polynomial groups.

References

[1] P. Wizinowich, "Adaptive optics in astronomy*". Contemporary Physics*, Vol. 56, No. 4, PP.1-19, 2015. DOI:10.1080/00107514.2015.1041765

[2] K. Niu and C. Tian, "Zernike polynomials and their applications", *Journal of Optics,* Vol. 24, No. 12, PP:1-54, 2022. DOI: 10.1088/2040-8986/ac9e08

[3] R. Navarro, J. L. López, J. A. Díaz, and E.r P. Sinusí, "Generalization of Zernike polynomials for regular portions of circles and ellipses", *Optics Express*, Vol. 22, Issue 18, pp. 21263-21279, 2014. https://doi.org/10.1364/OE.22.021263

[4] [A. J. E. M. Janssen, "Extended Nijboer–Zernike approach for the computation of optical point-spread functions", Journal of the Optical Society of America A, Vol. 19, Issue 5, pp. 849-857, 2002. https://doi.org/10.1364/JOSAA.19.000849

[5] R. N. Hassan, H.S. Ali, and W.H. Wadee, "Computer Simulation for the Effects of Optical Aberrations on Solar Images Using Karhunen-Loeve Polynomials", *Iraqi Journal of Science*, Vol. 62, No. 7, PP. 2463-2473, 2021. DOI: https://doi.org/10.24996/ijs.2021.62.7.35

[6] M. Segel, and S. Gladysz, "Optimal, blind-search Modal wave-front correction in atmospheric turbulence. Part I: simulations". *Optics Express*, Vol. 29, No. 2, PP. 805-820, 2021. https://doi.org/10.1364/OE.408682

[7] S. Wu, Yi Zheng and Y. Geng, "Time-Varying Statistics Identification of Nonstationary Random Fluctuating Pressure via Orthogonal Polynomial Representation and Karhunen–Loève Expansion". Journal of Aerospace Engineering, Vol. 36, Issue 6, PP. 04023081-20, 2023. https://doi.org/10.1061/JAEEEZ.ASENG-4672

[8] R. N. Hassan, "Atmospheric Turbulence Parameters Deduced from Vertical Profile of Cn2". *Iraqi Journal of Science,* Vol. 65, Issue 10, PP. 6070 – 6078, 2024. DOI:10.24996/ijs.2024.65.10(SI).14

[9] H. S. Ali, "Performance Estimation of Solar Imagery Using Different Types of Atmospheric Turbulence Models", *Iraqi Journal of Science*, Vol.64, No. 7, PP: 4579-4590, 2023. https://doi.org/10.24996/ijs.2023.64.7.43

[10] B. Barakat and J. W. Beletic, "Influence of atmospherically induced random wave-front on diffraction imagery: a computer simulation model for testing image reconstruction algorithms". *Journal of the Optical Society of America A*, Vol. 7, Issue 4, PP. 653-671, 1990. https://doi.org/10.1364/JOSAA.7.000653.

[11] H. M. Ozaktas, and M. A. Kutay, "Optical information processing: A historical overview", *Digital Signal Processing*, Vol. 119, pp:103248-14,2021. https://doi.org/10.1016/j.dsp.2021.103248

[12] B. D. Guenther, "Modern Optics Simplified", 1st Edition, *Oxford University Press*, UK, pp. 299-303, 2020.

[13] T. Yang, Y. Xu, H. Tian, D. Die, Q. Du, B. Zhang, and Y. Dan, "Propagation of partially coherent Laguerre Gaussian beams through inhomogeneous turbulent atmosphere". *Journal of the Optical Society of America A***,** Vol. 34, Issue 5, PP. 713-720, 2017. https://doi.org/10.1364/JOSAA.34.000713

[14] S. I. Taleb, C. Neipp, J. Francés, A. Márquez, M. L. Álvarez, A. Hernández, S. Gallego, and A. Beléndez , "Validation of Fresnel–Kirchhoff Integral Method for the Study of Volume Dielectric Bodies". *Applied Sciences*, Vol.11, No. 9, PP. 3800, 2021. DOI: 10.3390/app11093800

[15] M. S. Hernandez, H. V. Leal, L. H. Martinez, U. A. F. Nino, V. M. J. Fernandez, A. L. Herrera-May, R. C. Sheissa, R. C. A. Lazaro, and G. D. Arango, "Approximation of Fresnel Integrals with Applications to Diffraction Problems". *Mathematical Problems in Engineering,* Vol. 2018, Article ID 4031793, PP. 1-13, 2018. https://doi.org/10.1155/2018/4031793

[16] U.E. Jallod, "Simulations of Four Types of Optical Aberrations using Zernik Polynomials", *Iraqi Journal of Science*, Vol. 58, No. 1C, pp. 583-591, 2017. DOI: 10.24996/ijs.2024.65. 10(SI).14

[17] R. N. Hassan, and H.S. Ali, "performance estimation and system modeling for refractive index structure constant Cn2". *Karbala International Journal of Modern Science*, Vol. 9, No. 2, PP. 178-186, 2023. https://doi.org/10.33640/2405-609X.3291

[18] M. R. Chatterjee, and F. Mohamed, "Modeling of Power Spectral Density of Modified von Karman Atmospheric Phase Turbulence and Acousto-Optic Chaos Using Scattered Intensity Profiles Over Discrete Time Intervals", *Proceedings of the SPIE*, Vol. 9224, PP: 922404-16, 2014. DOI:10.1117/12.2065421

[19] A. O. Pérez, J. V.Hernández, R. M. H. Cuspinera, R. V. Mendoza, I. F.Tapia, S. T.López, M. O. Gutiérrez, J. B. R. Limón, and E. L. P. Lee, "Overlapping waves with random amplitude and phase". Proceedings Volume 11306, Practical Holography XXXIV: Displays, Materials, and Applications, Vol. 113060Q, 2020. https://doi.org/10.1117/12.2544990

[20] P. Daniel, "Experimental Characterization of Atmospheric Turbulence Supported by Advanced Phase Screen Simulations". *Ph.D. thesis, University of Maryland, College Park, United States*, pp. 39-51, 2020.

[21] D. Wegner, "Imaging Simulation Of Atmospheric Turbulence Based On Phase Screen Methods," *Ph.D. thesis, Institut für Meteorologie und Klimaforschung – Atmosphärische Spurenstoffe und Fernerkundung (IMK-ASF)*, PP. 75-83, 2022.

[22] A. Muschinski, "Phase-factor spectra of turbulent phase screens". *Journal of the Optical Society of America A***,** Vol. 38, Issue 9, PP. 1339-1348, 2021. https://doi.org/10.1364/JOSAA.429928

[23] A. P. Daniel, "Experimental Characterization of Atmospheric Turbulence Supported by Advanced Phase Screen Simulations", *Ph.D. thesis*, University of Maryland, College Park, United States, 2020.

[24] H. Y. Zhang, Y. Zhou, and F.Y. Li, "An Automatic Method for Generating Symbolic Expressions of Zernike Circular Polynomials". *IEEE Access*, Vol. 11, No. 6, PP. 56481-56493, 2023. https://doi.org/10.1109/ACCESS.2023.3283028

[25] D. Nguyen, K. Nguyen, B. X. Cao, V. Tran, T. Vu, and N. Bui ," Modal Reconstruction Based on Arbitrary High-Order Zernike Polynomials for Deflectometry", Mathematics, Vol. 11, No. 18, PP. 3915-3927, 2023. DOI: 10.3390/math11183915

[26] H. S. Ali, "Numerical Simulation of Solar Granulation Dynamics Using Optical Correction Techniques". *Iraqi Journal of Science*, Vol. ;66, No.4, PP1717-1728, 2025. doi:10.24996/ijs.2025.66.4.28

[27] A. Vyas, M. B. Roopashree, and B. R. Prasad, "Optimizing the modal index of Zernike polynomials for regulated phase screen simulation", *Proceedings of SPIE - The International Society for Optical Engineering*, Vol. 7736, 2010. DOI:10.1117/12.856816

[28] P. Bauweraerts, and J. Meyers, "Study of The Energy Convergence of The Karhunen-Loeve Decomposition Applied to The Large-Eddy Simulation of A High-Reynolds-Number Pressure-Driven Boundary Layer". *Physical Review Fluids*, Vol. 5, Issue 11, PP. 1-11, 2020. https://doi.org/10.1103/PhysRevFluids.5.114603

[29] S. Wu, Y. Zheng, and Y. Geng, "Time-Varying Statistics Identification of Nonstationary Random Fluctuating Pressure via Orthogonal Polynomial Representation and Karhunen–Loève Expansion". *Journal of Aerospace Engineering*, Vol. 36, No. 6, PP. 04023081- 12, 2023. https://doi.org/10.1061/JAEEEZ.ASENG-4672

[30] S. S. Bhairannawar, S. Sarkar, and K. B. Raja , "FPGA Implementation of Optimized Karhunen–Loeve Transform for Image Processing Applications". *Journal of Real-Time Image Processing*, Vol 17, No. 6, PP. 357–370, 2020. DOI:10.1007/s11554-018-0776-x

[31] C. C. Wilcox, S. R. Restaino, S.W Teare, and T. Martinez, "Adaptive optical system testbed with karhunen-loeve polynomial based method for simulating atmospheric turbulence". *Patent*, 2014. https://patents.justia.com/patent/20130201542

[32] B. B. Ren, "Karhunen-Loève data imputation in high-contrast imaging". *Astronomy and Astrophysics*, Vol. 679, Issue A18, PP. 1-8, 2023. https://doi.org/10.1051/0004-6361/202347354

[33] B. Guan, H. Yu, W. Song, and J. Choi, "Spatial Property of Optical Wave Propagation through Anisotropic Atmospheric Turbulence". *Wireless Communications and Mobile Computing,* Vol. 2021, Article ID 5519786, 2021. https://doi.org/10.1155/2021/5519786

[34] M. Carbillet and A. Riccardi, "Numerical modeling of atmospherically perturbed phase screens: new solutions for classical fast Fourier transform and Zernike methods", *Applied Optics*, Vol. 49, Issue 31, pp. G47-G52, 2010. https://doi.org/10.1364/AO.49.000G47